Coherent-state multipole moments in electron-hydrogen impact excitation

Yehuda B. Band*
Argonne National Laboratory, Argonne, Illinois 60439
(Received 22 August 1978)

We present results of various model calculations for the density-matrix elements of hydrogen excited by electron impact. These density-matrix elements are discussed in terms of expectation values of physically understandable observable multipole moment operators and their time derivatives, thereby enabling us to isolate and understand central features of the collision dynamics hidden in the off-diagonal density-matrix elements. The strengths and weaknesses of these various scattering models, including plane-wave Born, distorted-wave Born, Glauber, classical trajectory, quasiclassical close-coupling, and close-coupling approximations are pointed out. The effects of angular momentum barriers, the impulsive nature of excitation, the mixing and splitting of degenerate energy eigenstates of the final state manifold, and the various ranges and times of the interactions occurring durng the collision are described. We observe that perturbative scattering models are inappropriate to describe certain of these multipole, even at very high energies. Experiments which determine these multipole-moment parameters are discussed.

I. INTRODUCTION

The study of collision phenomena has, to a great extent, been restricted to the determination of cross sections. For example, in perhaps one of the simplest collision systems, electron-hydrogen atom scattering, the theoretical and experimental determinations of cross sections for elastic scattering, excitation, and ionization have been of continuous interest since the early days of atomic physics. However, scattering amplitudes contain additional information (their phases) concerning the collision processes. In this paper we analyze this additional information concerning the nature of the collision dynamics in terms of a recently developed physically understandable parametrization of the scattering amplitudes[1] and compare several calculational techniques for treating the collision dynamics for electron-hydrogen impact excitation.

It is important to note that we stress the need for a physically understandable parametrization of this information. The amplitudes contain a full description of the collision. However, these complex numbers, except for their magnitudes, are difficult to understand and interpret in terms of a physical picture of the collision dynamics. Considerable insight is gained when the coherently excited state of the system is described by its multipole moments and multipole-moment time derivatives. These parameters are easily visualized quantities which improve our perception of the nature of the final state and allow a greater understanding of the collision dynamics.

In Sec. II we briefly review the multipole moment representation of the final state for an electron hydrogen atom system after a collision event has occurred. In Sec. III we present the results of calculations for electron excitation of the hydrogen atom using various approximate collision models. I describe the energy and angular dependence of the coherence multipole moments and illucidate the collision mechanisms responsible for these behaviors. The deficiencies and the relative strengths of these collision models are pointed out. Predictions of these various scattering theory calculations for experiments which determine the coherence multipole parameters are given in Sec. IV. In Sec. V a summary and conclusion are presented.

II. COHERENT MULTIPOLE PARAMETERS

We first discuss electronic excitation of hydrogen to the $n=2$ state,

$$e+\mathrm{H}(1s)\rightarrow e'+\mathrm{H}(n=2), \tag{2.1}$$

and let us initially neglect spin. The coherently excited $n=2$ state may be written as a linear combination of standard orbital angular momentum states of $n=2$ (incident electron direction is taken as the z axis),

$$|\psi_{ex}\rangle=\sum_{lm}A_{nlm}(E_e,\Omega_e)|nlm\rangle\,. \tag{2.2}$$

The magnitude squared of the ampltidues A_{nlm} are the probabilities for producing the states (nlm) with electron energy E_e and scattering angle Ω_e. To exploit the symmetry properties of the collision it is convenient to discuss the excited state in terms of the density matrix[2]

$$\begin{aligned}\rho&=|\psi_{ex}\rangle\langle\psi_{ex}|\\&=\sum_{lm}\sum_{l'm'}A_{nlm}(E_e,\Omega_e)A^{*}_{nl'm'}(E_e,\Omega_e)|nlm\rangle\langle nl'm'|\\&=\sum_{lm}\sum_{l'm'}\rho_{lm,l'm'}(E_e,\Omega_e)|nlm\rangle\langle n'l'm'|\,,\end{aligned} \tag{2.3}$$

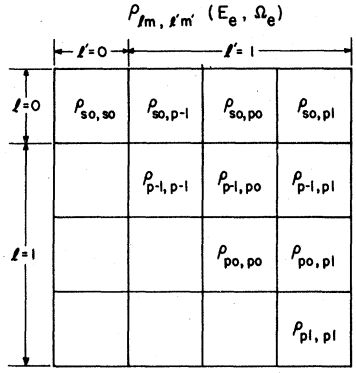

FIG. 1. Density-matrix representation for the $n=2$ manifold, $\rho_{lm,l'm'}(E_e,\Omega_e)=\langle n=2,l\,m|\,\rho(E_e,\Omega_e)\,|n=2,l',m'\rangle$.

thus defining $\rho_{lm,l'm'}(E_e,\Omega_e)$. Figure 1 shows all the elements of this density matrix for the $n=2$ state and contains 16 elements. The four diagonal elements are simply probabilities, but the twelve numbers comprising the off-diagonal elements (ρ is Hermitian) contain additional information and are more difficult to understand and interpret physically.

The average value of an operator Q is given by

$$Q=\mathrm{Tr}[\rho Q]. \tag{2.4}$$

Table I lists the relationships between the density matrix elements for the $n=2$ manifold and the average values of the multipole-moment operators and their time derivative operators $\dot{Q}=i[H,Q]$, defined by Gabrielse and Band.[1,3] (Actually we use linear combinations of the multipole-moment operators here.) Subscripts of the expectation values in Table I indicate that only part of the $n=2$ density matrix is used in taking the expectation value, namely the block of the density matrix identified by the subscript.

TABLE I. Multipole moments for $n=2$.

$\langle 1\rangle_s=\rho_{s0,s0}$
$\langle 1\rangle_p=\rho_{p1,p1}+\rho_{p0,p0}+\rho_{p-1,p-1}$
$\langle x\rangle=3\sqrt{2}\ [\mathrm{Re}(\rho_{s0,p1})-\mathrm{Re}(\rho_{s0,p-1})]$
$\langle y\rangle=3\sqrt{2}\ [\mathrm{Im}(\rho_{s0,p1})-\mathrm{Im}(\rho_{s0,p-1})]$
$\langle z\rangle=-6\,\mathrm{Re}(\rho_{s0,p0})$
$\langle \dot{x}\rangle=C\ [-\mathrm{Im}(\rho_{s0,p1})+\mathrm{Im}(\rho_{s0,p-1})];\ C=4.5\times10^{-6}$
$\langle \dot{y}\rangle=C\ [\mathrm{Re}(\rho_{s0,p1})+\mathrm{Re}(\rho_{s0,p-1})]$
$\langle \dot{z}\rangle=C\ \sqrt{2}\ [\mathrm{Im}(\rho_{s0,p0})]$
$\langle L_x\rangle=\sqrt{12}\ [\mathrm{Re}(\rho_{p0,p1})+\mathrm{Re}(\rho_{p0,p-1})]$
$\langle L_y\rangle=\sqrt{12}\ [\mathrm{Im}(\rho_{p0,p1})-\mathrm{Im}(\rho_{p0,p-1})]$
$\langle L_z\rangle=\sqrt{6}\ (\rho_{p1,p1}-\rho_{p-1,p-1}$
$\langle 3z^2-r^2\rangle=12(\rho_{p1,p1}-2\rho_{p0,p0}+\rho_{p-1,p-1})$
$\langle xz\rangle=-6\sqrt{2}\ [\mathrm{Re}(\rho_{p0,p1})-\mathrm{Re}(\rho_{p0,p-1})]$
$\langle yz\rangle=-6\sqrt{2}\ [\mathrm{Im}(\rho_{p0,p1})+\mathrm{Im}(\rho_{p0,p-1})]$
$\langle x^2-y^2\rangle=-24\,\mathrm{Re}(\rho_{p1,p-1})$
$\langle xy\rangle=12\,\mathrm{Im}(\rho_{p1,p-1})$

For measurements of the excited state which do not determine the electron scattering angle, the angle averaged density matrix, given by

$$\begin{aligned}\rho&=\int|\psi_{ex}\rangle\langle\psi_{ex}|\,d\Omega_e\\&=\sum_{lm}\sum_{l'm'}\int d\Omega_e A_{nlm}(E_e,\Omega_e)\\&\qquad\times A^*_{nl'm'}(E_e,\Omega_e)\,|nlm\rangle\langle nl'm'|\\&=\sum_{lm}\sum_{l'm'}\langle nlm|\rho|nl'm'\rangle\,|nlm\rangle\langle nl'm'|,\end{aligned}\tag{2.5}$$

must be used in Eq. (2.4). It is this context, involving a mixture of pure quantum states, where the notion of the density matrix (or equivalently, the multipole moments) becomes essential. Such an angle averaged state is symmetric under rotations about the incident beam direction, and under reflections in any plane containing the beam direction. Because of these symmetries, the angle averaged density-matrix elements with $m\neq m'$ vanish, $\int d\Omega_e\rho_{lm,l'm'}(E_e,\Omega_e)=0$, and $\int d\Omega_e\rho_{lm,l'm'}=\int d\Omega_e\rho_{l-m,l'-m'}$. This leaves three probabilities along the diagonal for producing the s, $p0$, and $p1$ states, and one complex off-diagonal density-matrix element, $\rho_{s0,p0}=\int d\Omega_e\rho_{00,10}(E_e,\Omega_e)$.

It is difficult to determine even the sign of the real and imaginary parts of $\rho_{s0,p0}$, let alone the magnitudes, from considering the general properties of the collision mechanism. It is in this connection that the multipole-moment description of the density matrix plays a vital role. It is clear that the full information concerning the excited state is contained in $\rho_{lm,l'm'}(E_e,\Omega_e)$. However, as described in an earlier paper,[1] when the density-matrix elements are related to average values of position and angular momentum operators, and higher moments constructed from these operators, it is easier to interpret the density matrix elements physically. It therefore becomes easier to extract the information they contain regarding the nature of the collision. For example, the $n=2$ density matrix element $\rho_{s0,p0}$ is interpreted in terms of the average values of the position vector $\langle z\rangle$ and its time derivate $\langle\dot{z}\rangle$. This physical interpretation will enable us to understand central features of the dynamics of the collision process and allow us to point out the strengths and difficulties of the various scattering models.

The diagonal blocks in l, $l=l'$, of the density matrix could have been given solely in terms of products of angular momentum operators.[4] However, to provide a complete specification of the off-diagonal

blocks in $\mathfrak{L}$ as well as the diagonal blocks, an additional set of operators with even and odd behavior under parity and time reversal are needed. We have chosen the electric and magnetic multipole-moment operators as well as their time derivative operators. These operators have the proper behavior under rotations, parity, and time reversal transformations in order to completely specify the density matrix.

However, the expectation values of the time derivatives $\langle \dot{Q} \rangle$ vanish identically for *energy* degenerate energy levels. Thus the multipole-moment time-derivative operators must be modified for describing such coherently excited degenerate states. Nevertheless, average values of these operators provide a complete description of the density matrix for coherently excited states which are nearly degenerate. Thus the constant C, relating expectation values of $\langle \vec{x} \rangle$ to the density-matrix elements in Table I, is related to the energy differences of the $n=2$ nearly degenerate states. This difficulty with the time-derivative operators can be circumvented by taking products of multipole-moment operators with the correct behavior under rotations, parity, and time reversal. Operators such as

$$[Q_{k+1,q}\dot{z}]_{kq} + [\dot{z}Q_{k+1,q}]_{kq}, \tag{2.6}$$

where k, q denotes rotational properties of the tensors, and [ ] indicates the coupling to a specific tensorial representation, have the proper form and do not vanish when average values among degenerate states are taken. Such parametrizations will be discussed elsewhere.[3] Nevertheless, it is important to note that the multipole-moment operators of Table I have the advantage of being easy to relate to our intuitive ideas concerning classical position, velocity, and angular momentum variables. Another advantage of the multipole moments is that, unlike the density matrix elements $\rho_{lm,l'm'}$, they are independent of phase conventions of the spherical harmonics (here Y_{l0} are taken as real) and the radial wave functions [here $R_{nl}(r)$ are taken as positive near the origin].

The multipole-moment parametrization in Table I can clearly be extended to $n=3$ and higher states with a corresponding increased number of multipole moments and their derivatives. In what follows we shall plot the density-matrix elements directly (normalized as cross sections by a kinematical factor which relates the diagonal density matrix elements to cross sections), but we shall refer to the linear combinations of the density matrix elements which form the multipole moment expectation values for physical insight.

III. COMPARISON OF SCATTERING MODEL CALCULATIONS

We investigate the predictions of various scattering models for the density matrix of excited states of hydrogen produced by electron impact. First we describe briefly these models and the relevant physical concepts that they incorporate.

A. Plane-wave Born approximation (PWBA)

This approximation treats the interaction as an impulse to the hydrogen atom during which the bound electron has no time for rearrangement. The incident electron is described in terms of an incident plane wave, undistorted and unaffected by the presence of the target atom. After the impulsive transfer of momentum, the scattered electron is described by a plane wave with the asymptotic electron momentum and energy. Generally the PWBA cross sections are reliable for sufficiently high incident particle energy, since at high energy the incident and exit waves of the projectile electron are not strongly affected by the presence of the atom.

The reliability of PWBA at high energies is not nearly so good when used to calculate density matrix elements which are not cross sections, i.e., those not diagonal in l. We will show that even when the incident particle velocity is much larger than the internal velocity of the bound electron, the distortion of the projectile plane waves is very important in the calculation of coherence multipoles. Even more significant is the neglect in PWBA of the mixing of the nearly degenerate hydrogen states brought about by the projectile electron as it departs. Hence the transition amplitude phases produced by a first-order perturbation expansion of the transition amplitudes are not accurate. Keeping higher-order terms in the interaction potential $|\vec{x}-\vec{r}|^{-1}$, as in typical second Born approximations, will not significantly improve the results.

The PWBA amplitudes for excitation from the $1s$ state are given by

$$A_{nlm}(E_e, \Omega_e) = (2\pi)^{-3} \int\int d^3r_1 d^3r_2 \psi^*_{nlm}(\vec{r}_1) \times e^{i\vec{q}\cdot\vec{r}_2} |\vec{r}_1 - \vec{r}_2|^{-1} \psi_{1s0}(\vec{r}_1), \tag{3.1}$$

where $\vec{q}$ is the momentum transfer, $\vec{q} = \vec{k}_i - \vec{k}_f$. Notice that both the effective potential, which connects the initial and final states, and the initial $1s0$ state are invariant under simultaneous time-reversal transformation (T) and a parity transformation (P). All of the multipole moments and multipole-moment time derivatives produced by this potential from the $1s0$ state must therefore be in-

variant under PT transformations or vanish. Thus half of the off-diagonal multipole-moment parameters vanish identically according to PWBA, at all angles and energies. The off-diagonal density-matrix elements are either pure real or pure imaginary, depending upon their PT transformation characteristics. Another way of reaching the same conclusion is by observing that the only dynamical variable in PWBA is the momentum transfer vector $\vec{q}$, which is PT even. It is therefore not possible to construct a PT odd tensor in PWBA. Average values of all PT odd tensors must therefore vanish.

B. Distorted-wave Born approximation (DWBA)

The DWBA incorporates the distortion of the motion of the projectile electron due to the presence of the target into the calculation of the transition amplitudes. The plane waves in the initial and final channels of the PWBA are replaced by *distorted waves*. The excitation is once again considered to be impulsive. The bound states of the atom are treated as if they are unaffected by the presence of the external charge in the vicinity of the atom. The major deficiency of PWBA remains since the various nearly degenerate excited states are not further coupled by the interaction potential.

The DWBA transition amplitudes for excitation of the H target are given by

$$A_{nlm}(E_e,\Omega_e)=\int\int d^3r_1 d^3r_2 \psi^*_{nlm}(\vec{r}_1)\psi^{(-)*}_{k_f} \times (r_2)|\vec{r}_1-\vec{r}_2|^{-1}\psi_{1s0}(\vec{r}_1)\psi^{(+)}_{k_i}(\vec{r}_2)\,. \tag{3.2}$$

$\psi^{(+)}_{k_i}(r)$ is the wave function for the initial electron which evolves from the initial projectile electron state with momentum $\vec{k}_i$ in the presence of the static potential $U_i(r)$ of the ground-state hydrogen atom. $\psi^{(-)}_{k_f}$ is the outgoing plane wave distorted by the atomic potential $U_f(r)$. When exchange is included, this expression must be appropriately symmetrized.

We have performed numerical calculations with different choices of U_i and U_f with and without inclusion of static polarization potentials. We find that at electron energies above 100 eV all choices give similar results. At these energies the exchange contributions are small ($\leq 1\%$). For high angular momentum components of the wave functions ($L \geq 100$) which contribute to the transition amplitudes we employ an analytic approximation to the radial integrals, $\int_0^\infty F_L(kr)F_{L'}(kr)r^{-(l+1)}dr$, obtaining, aside from a Coulomb correction factor (which is unity for the hydrogen atom case considered here), the analytic Born approximation result.[5] For smaller angular momentum, the long-range part of the radial integrals (the parts without an exponentially decaying radial factor), $\int_{R_{\max}}^\infty F_L(kr)F_{L'}(k_f r)r^{-(l+1)}dr$, is treated using an asymptotic expansion method similar to that of Belling.[6] At energies above about 100 eV, the scattering phase shifts are small, so that $\psi^{(-)}_{k_f}$ and $\psi^{(+)}_{k_i}$ deviate little from plane waves, and the amplitudes in the DWBA approximation are close to the PWBA amplitudes.

Calhoun, Madison, and Sheldon[7] have published $e-\mathrm{H}$ $n=2$ differential and integral cross sections using DWBA. Our $n=2$ cross-section results all agree with their results as corrected in Ref. 7. In this paper we focus only upon the much less studied coherence multipoles.

C. Close-coupling approximation (CCA)

The CCA is a much better approximation than either PWBA and DWBA, largely because it is not a perturbation expansion in powers of the interaction potential. As already pointed out, an essential feature of the excitation of H atoms by electron impact is the ability of the projectile to *strongly* mix the nearly degenerate levels of the hydrogen atom. All bound states are fully coupled to all orders in the interaction r_{12}^{-1}. This accounts not only for the mixing of degenerate levels, but their distortion as well. Furthermore, the CCA allows for distortion of the incident particle motion, resonance phenomena, and a systematic treatment of exchange.

The CCA involves expansion of the wave function for the two-electron system for each initial channel in terms of wave functions for the bound one-electron atom ψ_i, times continuum wave functions θ_i (whose form will be specified momentarily), plus bound-state wave functions for the two-electron system Φ_j.[8,9] The latter functions represent resonance states formed in the collision. Thus for each channel i', the wave function becomes

$$\Psi^{i'}(1,2)=\sum_{i=1}^{I}\psi_i(1)\theta_i(2)+\sum_{j=1}^{J}\Phi_j(1,2)C_j\,. \tag{3.3}$$

The full Schrödinger equation is then solved for the continuum wave functions θ_i and C_j. The details of the calculational methods are discussed in Refs. 8 and 9, hence we will not labor them here.

The CCA results reported here were computed using the published $1s$-$2s$-$2p$ coupled R matrices of Burke, Schey, and Smith[8] which were computed for partial waves $0 \leq L \leq 7$. For larger-L partial waves we have used PWBA partial-wave amplitudes (a serious liability). No bound-state functions Φ_j were included. Also, no continuum channels for $\psi_i(1)$ were included. Since many continu-

um channels are open this may be a serious liability.

D. Glauber approximation

The Glauber approximation assumes that the projectile electron wave function can be treated in a WKB-like fashion, that the electron motion is along a straight line trajectory, and that the momentum transfer to the electron is perpendicular to the trajectory. The interaction potential is not treated perturbatively. Because of the WKB-like nature of this approximation, the Glauber amplitude contains the potential as an argument of an exponential. The Glauber amplitude is given by

$$A_{nlm}(E_e,\Omega_e)=(2\pi)^{-3}\int\int d\vec{r}_1 d\vec{r}_2\, e^{i\vec{q}\cdot\vec{r}_2}V(\vec{r}_1,\vec{r}_2)\times\exp\left[-i\int_{-\infty}^{z}V(\vec{r}_1,\vec{r})\,dr_z\right]\times\psi^*_{nlm}(\vec{r}_1)\psi_{1s0}(\vec{r}_1), \quad (3.4)$$

where $\vec{q}$ is the momentum transfer, $V=|\vec{r}_{12}|^{-1}-r_2^{-1}$, and the z axis is taken along the straight-line trajectory perpendicular to $\vec{q}$. Several derivations of the Glauber (and Eikonal) amplitudes have been published.[10] However, the physical implications of these approximations are not completely clear. The Glauber amplitudes we use were calculated for us by Chan.[11]

E. Classical-trajectory approximation (CTA)

As discussed in the previous paragraphs, the central features of the e-H interaction which are neglected in the PWBA are the mixing of the nearly degenerate hydrogenic levels by the projectile and the distortion of the projectile motion from plane waves. The CCA incorporates both these aspects of the collision dynamics. However, at sufficiently high energies ($\gtrsim$200 eV) the CCA is expensive to calculate. To complement the low-energy CCA, yet incorporate both of these features, we use a CTA similar to the approximation used in nuclear physics to describe Coulomb excitation.[5] For a given impact parameter, the projectile electron trajectory $\vec{R}(t)$ is calculated using a suitable atomic potential (see below). The atom sees the time-dependent potential due to the projectile electron following its classical trajectory. The time-dependent Schrödinger equation for the amplitudes of the atomic states $a_j(t)$, $j=1,\ldots,I$,

$$ia_j(t)=\sum_{k=1}^{I}V_{jk}(t)\exp[-i(E_K-E_j)t]a_K(t), \quad (3.5)$$

where

$$V_{jk}(t)=\int d^3r\psi_j^*(r)[|\vec{R}(t)-\vec{r}|^{-1}-R^{-1}(t)]\psi_k(r) \quad (3.6)$$

is solved for $\{a_j(t=\infty)\}$ for each impact parameter, with proper boundary condition for the amplitudes at $t=-\infty$. The transition amplitude $(i\to j)$ is given by

$$A_{j,i}(E_e,\Omega_e)=\sum_{b(\theta_e)}\left[\frac{b(\theta_e)}{\sin\theta_e}\left|\frac{db}{d\theta_e}\right|\right]^{1/2}e^{2i\delta_b}a_{ji}(t=\infty), \quad (3.7)$$

where δ_b is the classical (WKB) phase shift for trajectory with impact parameter $b(\theta)$. In the electron-atom collision, the potential for the relative motion is monotonic, so there is only one trajectory $b(\theta_e)$ for any scattering angle θ_e. In making the classical trajectory approximation we neglect diffraction effects (i.e., we neglect the fact that all angular momenta, and therefore all impact parameters, contribute to scattering into a given angle θ_e). Furthermore, it is well known that extremely forward scattering is poorly represented by classical trajectory calculations.[12] These deficiencies are less important in considering angle-integrated results, because the angular integration tends to wash out diffraction effects and compensates by weighting the small angles with $\sin\theta_e$.

The criteria for validity of the CTA[13,14] clearly include the necessity that the trajectories for the relative motion in the different internal states of the atom be comparable. This is the case when the kinetic energy of relative motion is large compared with the *differences* between the static potentials for the different internal states. We found that the amplitudes were insensitive to the choice between trajectories calculated using the initial- or final-state atomic potential.

In the calculations we report here, we used a $1s$-$2s$-$3s$-$3p$-$3d$ basis. Including higher excited states does not significantly affect the reported results. The numerical Schrödinger equation was solved using a scaling integration grid GEAR method. Possibilities for treating continuum states via Sturmium bases are presently under study. Also being developed are methods which incorporate diffraction effects into the treatment of the relative motion degrees of freedom.[13,14] This generalization of the CTA amounts to making a quasiclassical approximation to the full close-coupling equations. This improved approximation, to be called quasiclassical close-coupling approximation (QCCA) removes a serious liability of the CTA in the *angular distributions* for $\Delta M\neq 0$ transitions. The error in the CTA due to the large angle approximation for the spherical harmonics, which must be made to obtain the CTA from the QCCA, is particularly poor for $\Delta M\neq 0$ transitions.[13,14]

Our confidence in this approximation is bolstered by the fact that the CTA results extrapolate back to CCA results at lower energies. The CTA takes about a factor of ten less computing time than does the DWBA. This makes it possible to do various numerical experiments mentioned above and others discussed later. More importantly, the CTA incorporates the important features of the collision dynamics which are left out of the DWBA approach. It is important that the potential is *not* treated perturbatively. We thus have an approximation which incorporates the mixing (and the shift in energies) of the target states. Projectile distortion is incorporated by using curved trajectories.

F. Results using the various scattering models and qualitative physical interpretations

I present and compare the results of these various scattering models for electron–hydrogen-atom excitation to the $n=2$ and $n=3$ states. The energy- and angle-dependent features of the results will be used to point out the dynamical effects which give rise to these dependences.

We begin by presenting the energy-dependent trends of the multipole moments when the scattered electron is not detected. The collision symmetry for excitation permits five nonzero independent multipole moments (or density-matrix elements) for the $n=2$ states; $\langle 1\rangle_s=\rho_{2s}$, $\langle 1\rangle_p=\rho_{2p}$, $\langle 3z^2-r^2\rangle$, $\langle z\rangle$, $\langle \hat{z}\rangle$. Multipole moments not symmetric about the incident particle direction vanish. Furthermore, the magnetic dipole moment $\langle L_z\rangle$ vanishes because it is odd under reflections in any plane passing through the incident particle direction. For the $n=3$ states there are 15 independent nonzero angle-integrated multipole moments, as discussed earlier.

All of these multipole moments have common features in their energy dependence. Near threshold they rise sharply as a function of increasing energy. For those multipole moments involving nonzero angular momentum states, there is an additional angular momentum barrier to overcome in order to create the nonzero angular momentum state. All the multipole moments rise to a maximum magnitude and then fall off with increasing energy (perhaps after changing sign as in the case of the quadrupole moment $\langle 3z^2-r^2\rangle_{3p}$) due to the shorter effective interaction time of the projectile electron. These features are illustrated in all the figures of the energy dependence of the angle-integrated multipole moments.

A common feature of multipole moments which are PT even is that at sufficiently large energies, the PWBA and DWBA results are not significantly different from the results using nonperturbative methods such as Glauber and CTA. On the other hand, PT-odd multipole moments vanish in PWBA for all energies and are small in DWBA. Nonperturbative approximations yield results quite different from the first-order perturbation results. As an example, consider the $n=2$ electric dipole moment and electric dipole moment time derivative which are plotted as a function of energy in Fig. 2. The dipole moment $\langle z\rangle$ is zero at all energies according to the PWBA. The DWBA approximation gives a small dipole moment. This smallness is shown more clearly in Fig. 3, which plots $\tan^{-1}(\mathrm{Im}\rho_{s0,p0}/\mathrm{Re}\rho_{s0,p0})$, the phase of $\rho_{s0,p0}$. The PWBA phase in Fig. 3 is $-90°$. The DWBA phase is very nearly $-90°$. The values at low incident energies for the dipole moment and time derivative plotted in Fig.

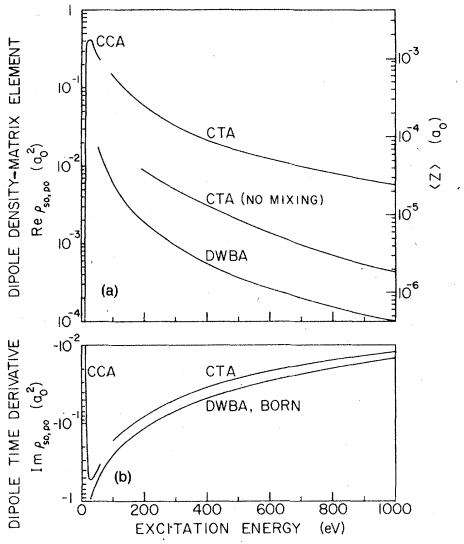

FIG. 2. (a) $n=2$ dipole density-matrix element $\mathrm{Re}\,\rho_{s0,p0}$ vs incident electron energy. Scale at right gives $\langle z\rangle$. (b) $n=2$ dipole time-derivative density-matrix element $\mathrm{Im}\,\rho_{s0,p0}$.

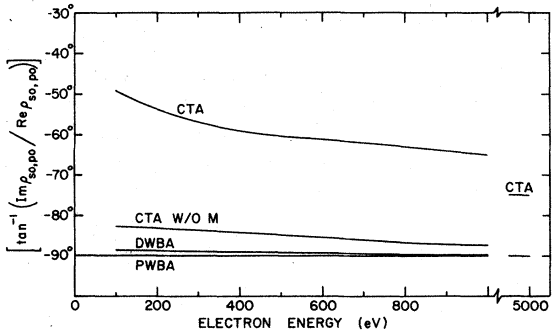

FIG. 3. Comparison of $\tan^{-1}[\mathrm{Im}\,\rho_{s0,p0}/\mathrm{Re}\,\rho_{s0,p0}]$ vs incident electron energy.

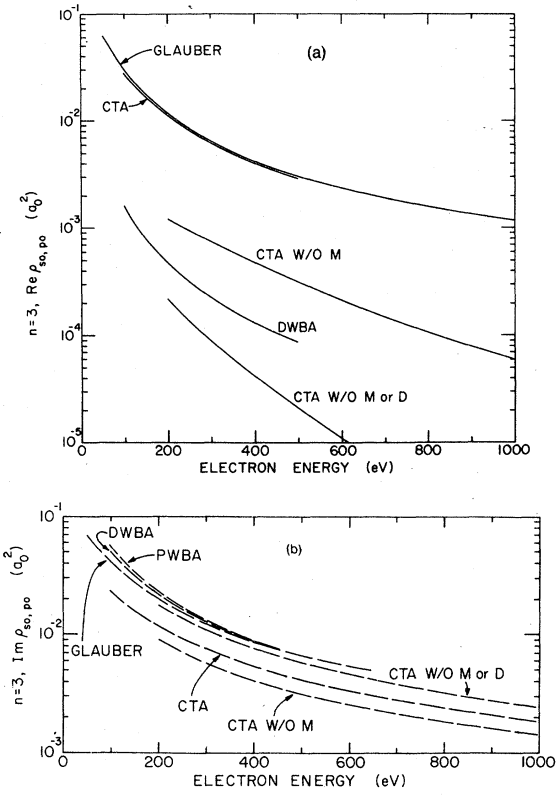

FIG. 4. (a) $n=3$ dipole density-matrix element $\mathrm{Re}\,\rho_{s0,p0}$ vs incident electron energy. (b) $n=3$ dipole time-derivative density-matrix element $\mathrm{Im}\,\rho_{s0,p0}$. Dashed curves indicate negative quantities.

2 are small. As already mentioned, this is partly due to the angular momentum barrier for creating the p state of the hydrogen atom near threshold. Since a dipole moment is possible only by having a superposition of different angular momentum states, and the p state is suppressed even more than the s state near threshold, the dipole moment is small. As the energy is increased above threshold these moments grow in magnitude. The CCA dipole moment is far from zero. In fact $\mathrm{Re}\rho_{s0,p0}$ is larger in magnitude than $\mathrm{Im}\rho_{s0,p0}$. At higher energies, where CCA R matrices are not available to us, we use the CTA. We find that the CTA results for $\rho_{s0,p0}$ (and for cross sections and other multipole moments) extrapolate smoothly to the low-energy CCA results.

The $n=3$ dipole moments and time derivatives show similar energy dependences. In Fig. 4 we plot the $n=3$ dipole-moment term $\mathrm{Re}(\rho_{s0,p0})$ and time-derivative term $\mathrm{Im}(\rho_{s0,p0})$. The time-derivative term as calculated in all the approximations are similar, whereas $\mathrm{Re}(\rho_{s0,p0})$ is very sensitive to the scattering model employed. A striking feature of Fig. 4(a) is the similarity of the CTA and Glauber results, especially when compared with the DWBA and PWBA (which is zero for all energies). The similarity of the dipole-moment time-derivative terms and disparity of the dipole-moment terms as calculated in the different approximations for sufficiently high energies are displayed in Figs. 5 and 6 for $n=3$, $\rho_{p0,d0}$ and $\rho_{p1,d1}$, respectively. In Fig. 5(b) we see that below about 400 eV the dipole-moment time-derivative term $\mathrm{Im}(\rho_{p0,d0})$ is very sensitive to the approximation used to calculate it, but at higher energies all the approximations yield similar results. Figure 6(a) shows that, contrary to the dipole-moment term, $\mathrm{Re}(\rho_{s0,p0})$, $\mathrm{Re}(\rho_{p1,d1})$ is radically different as calculated in the CTA and Glauber approximations.

As another example of these general features, we plot in Fig. 7 the energy dependence of the scattering-angle integrated electric-quadrupole moment $\mathrm{Re}\rho_{s0,d0}$ and its time derivative $\mathrm{Im}\rho_{s0,d0}$. The PWBA time derivative $\mathrm{Im}\rho_{s0,d0}$ is zero for all energies. Again the DWBA gives small deviations from the Born result. At low energy (lower than the ener-

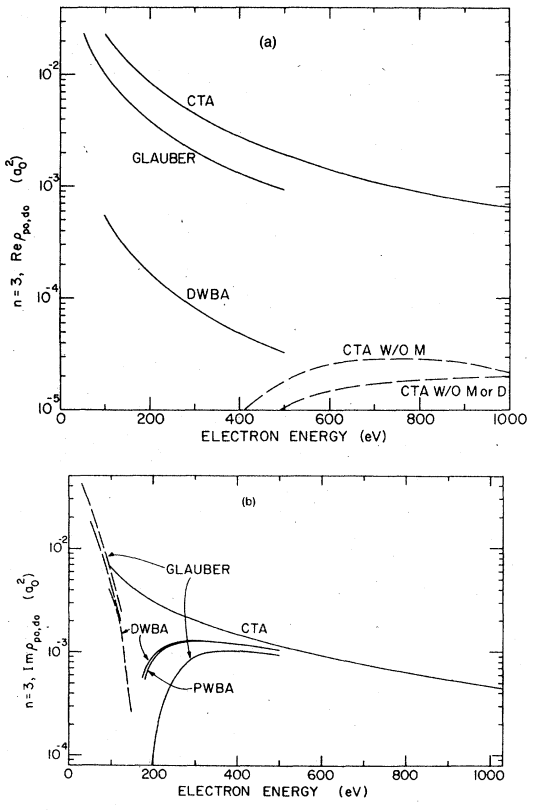

FIG. 5. (a) $n=3$ dipole density-matrix $\mathrm{Re}\,\rho_{p0,d0}$, vs incident electron energy. (b) $n=3$ dipole time-derivative density matrix element $\mathrm{Im}\,\rho_{p0,d0}$. Dashed curves indicate negative quantities.

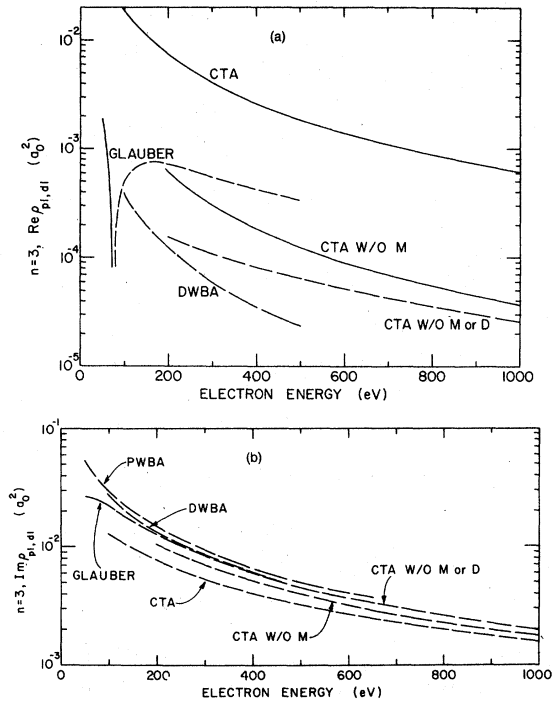

FIG. 6. (a) $n=3$ dipole time-derivative density-matrix element Re $\rho_{p1,d1}$ vs incident electron energy. (b) $n=3$ dipole time-derivative density-matrix element Im $\rho_{p1,p1}$. Dashed curves indicate negative quantities.

gies considered in Fig. 7) the d state is further suppressed by the angular momentum barrier so that near threshold for the $n=3$ excitation, $\rho_{s0,d0}$ is small. A rapid rise above threshold is again present. Even at the highest energies the CTA result for $\mathrm{Im}\rho_{s0,d0}$ is not converged to the PWBA or DWBA values. The Glauber values are plotted in Fig. 7 for $\mathrm{Re}\rho_{s0,d0}$ and $\mathrm{Im}\rho_{s0,d0}$. The Glauber values for $\mathrm{Im}\rho_{s0,d0}$ differ from PWBA character dramatically. The $\mathrm{Re}\rho_{s0,d0}$, for which the PWBA symmetry allows a nonzero value is similar in all the calculated approximations for energies above 200 eV. This is reminiscent of the dipole time derivatives $\mathrm{Im}\rho_{s0,p0}$, $\mathrm{Im}\rho_{p0,d0}$, and $\mathrm{Im}\rho_{p1,d1}$.

Other quadrupole-moment contributions to the $n=3$ state are proportional to $[\rho(3p1)-\rho(3p0)]$ and $[2\rho(3d2)-\rho(3d1)-\rho(3d0)]$. These PT-even moments are plotted as a function of energy in Figs. 8 and 9 for DWBA, Glauber, and CTA. Again we find that the disparity of the results below 300 eV is quite large, but for sufficiently high-incident electron energies the differences between the results are not substantial.

In order to determine the nature of the radically different behavior of the PT-even and -odd multipole moments we perform a numerical experiment with the CTA. By repeating the CTA calculation

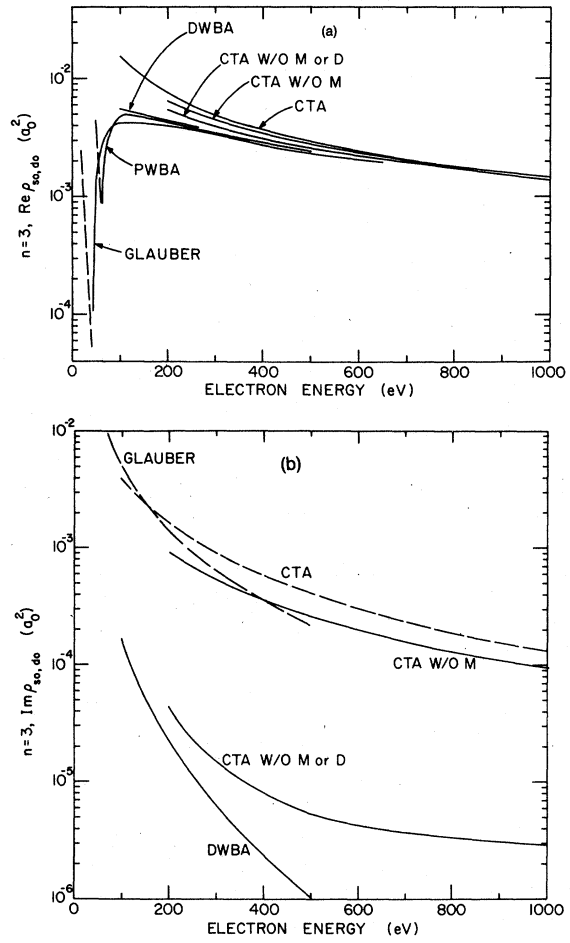

FIG. 7. (a) $n=3$ quadrupole density-matrix element Re $\rho_{s0,d0}$ vs incident electron energy. (b) $n=3$ quadrupole time-derivative density- matrix element Im $\rho_{s0,d0}$. Dashed curves indicate negative quantities.

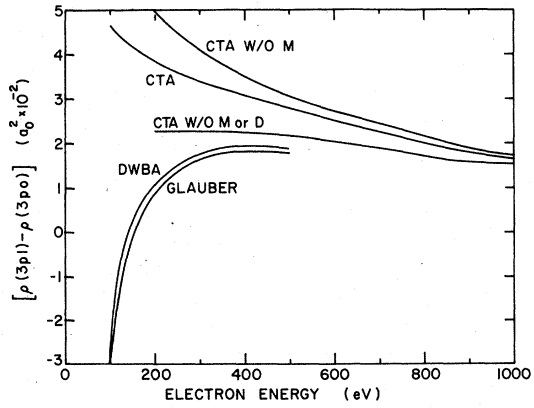

FIG. 8. Contribution to the $n=3$ quadrupole moment from the diagonal density-matrix elements (cross sections) of the $3p$ states $[\rho_{p1,p1}-\rho_{p0,p0}]$. See Table I (that factor 12 is different from the $n=2$ result. Also, for angle integrated cross sections $\rho_{p1,p1}=\rho_{p-1,p-1}$).

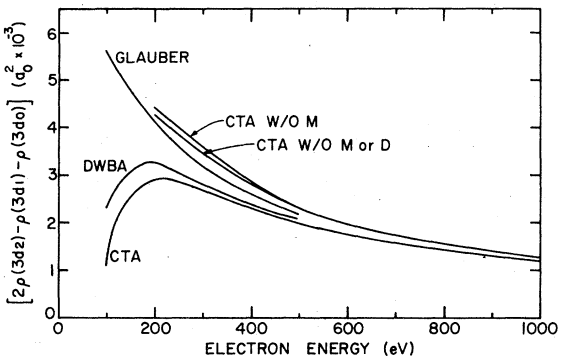

FIG. 9. Contribution to the $n=3$ quadrupole moment from the diagonal density-matrix elements (cross sections) of the $3d$ states, $[2\rho_{d2,d2}-\rho_{d1,d1}-\rho_{d0,d0}]$.

setting terms in the Hamiltonian which mix the degenerate excited states equal to zero, we find that the $n=2$ $\mathrm{Im}\rho_{s0,p0}$ (and the cross sections PT even) are not radically affected, but the $n=2$ dipole moment $\mathrm{Re}\rho_{s0,p0}$ (PT odd) is orders of magnitude closer to the PWBA and DWBA values. We conclude that the dipole moment is very sensitive to the final-state mixing of the degenerate energy eigenstates of the atom brought about by the scattered electron as it leaves the hydrogen atom (such calculations are denoted in the figures by CTA W/O M). If in addition we set to zero the energy shifts in the various states induced by the presence of the scattered electron (we call this a distortion effect), we obtain an $n=2$ dipole moment $\mathrm{Re}\rho_{s0,p0}$ even smaller than the DWBA value, and the dipole time derivative $\mathrm{Im}\rho_{s0,p0}$ approaches the PWBA and DWBA values (see Fig. 2) (such calculations are denoted in the figures by CTA W/O M or D). Thus the mixed-l coherence multipole moment $\rho_{s0,p0}$ is sensitive not only to the mixing of the degenerate atomic states, but also to the distortions of the target bound states produced by the projectile electron. Since both final-state mixing and target distortion are large effects occuring between nearly degenerate states, Born and similar perturbation methods are completely inappropriate to describe such phenomena. Even at an incident electron energy of 5 000 eV we see from Fig. 3 that the phase of the $\rho_{s0,p0}$ multipole moment is not converged to the DWBA value, and shows very poor convergence trends as the energy is increased further. The very long range of the interactions responsible for these phenomena insure their manifestation even at very high energies. These features are corroborated in all the energy-dependent multipole moments shown in Figs. 2–9.

We now turn to investigate the angular dependence of the coherence multipole moments at given fixed electron energy. A word of caution is in order concerning the limitations of the approximations as far as angular distributions are concerned. At

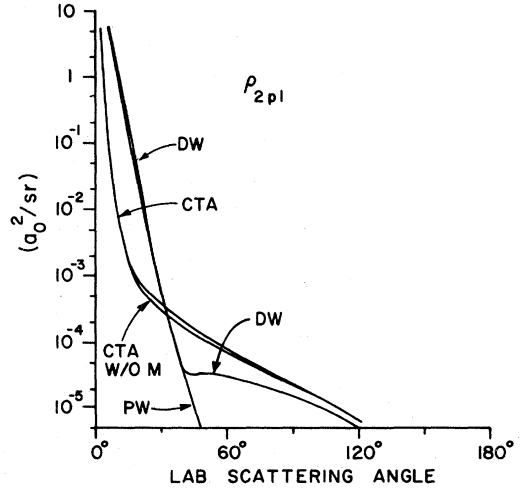

FIG. 10. $n=2$ diagonal density-matrix element (cross section) $\rho_{p1,p1}$ vs electron scattering angle for 200-eV incident electron energy.

large scattering angles, all the approximations employed here have severe limitations. The large angle scattering region contains the strongly interacting portion of the scattered flux. Perturbation methods are least capable of describing this region of strong interactions. Furthermore, a basis set description of this strongly interacting region which truncates all but the lowest-energy basis states must be viewed with caution. The part of the scattered flux which would go into the higher excited states and into ionization is not properly treated with a truncated expansion. The region of strong interaction may have a substantial portion of the flux in this excitation region. All the methods employed herein are basis-state methods and

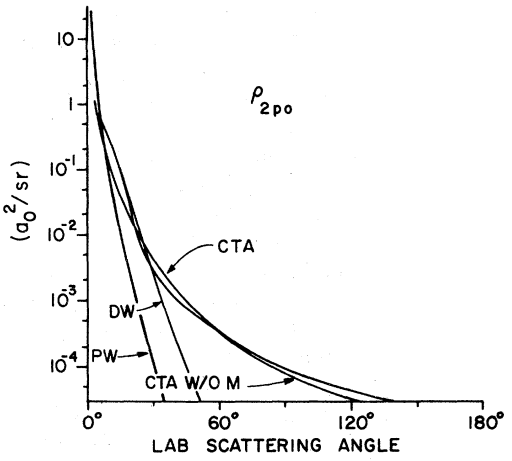

FIG. 11. $\rho_{p0,p0}$ cross section. See Fig. 10 caption.

must therefore be viewed with a certain skepticism.

An important model-dependent feature of the CTA is its incorrect treatment of the small-angle region of the angular distributions.[13] This is particularly true of multipole moments involving nonzero azimuthal quantum numbers, where the angular distributions must vanish, and where the CTA results may not have this property. The origin of this difficulty is the large angle approximation to the spherical harmonics made to obtain the CTA result. Figure 10 illustrates this difficulty in the $2p1$ cross section. Figure 11 shows the $2p0$ cross section, illustrating that a large disparity at small angle for $\Delta m = 0$ transitions is not present. As already mentioned, the QCCA corrects this liability.[13,14]

There are many common features in the angular distributions we are about to display. The angular distributions are all forward peaked. However, those moments involving nonzero azimuthal quantum numbers must vanish at 0° (and 180°). Such moments (i.e., σ_{2p1}, $\langle z \rangle_{p1,d1}$, etc.) are observed to rise in magnitude very rapidly away from 0°. These features are present in all the computed angular distributions regardless of scattering model.

There are clear model-dependent features of the multipole moments. All the multipole moments calculated using PWBA are expected to be poor at large momentum transfer (i.e., large angles). Cross sections calculated using PWBA are orders of magnitude smaller at large angle than other approximations. DWBA and CTA (even without final-state coupling) fill in the large angle cross section. In general, the PT-even multipole moments as calculated in the various approximations are similar except at very large and small scattering angles. As already noted, a feature of the DWBA is the vanishing of the PT-odd multipole moments for all angles. For the PT-odd moments the nonperturbative results are vastly different from PWBA and DWBA.

Figure 12 shows the angular dependence of the $n=2$ dipole moment $\langle z \rangle$ and its time derivative $\langle \dot{z} \rangle$. Recall that the PWBA $\mathrm{Re}\rho_{s0,p0}$ vanishes for all angles. The nonzero DWBA result indicates the angular distribution of the dipole moment induced in the hydrogen atom by virtue of the distortion (deflection) of the motion of the projectile electron due to the presence of the target from the plane-wave character. Thus the DWBA predicts a change of sign of the dipole moment due to this projectile electron deflection. The CTA without mixing or (target) distortion predicts a similar angular distribution. With the inclusion of these effects the bound $n=2$ electron cloud (once the $n=2$ states are excited) is forced away from the projectile electron, thus contributing an additional contribution to the dipole moment.

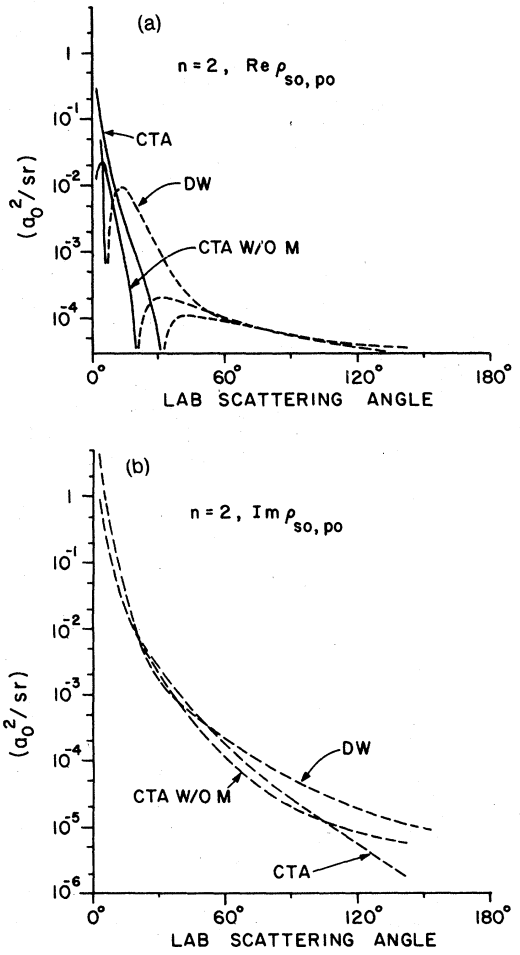

FIG. 12. (a) $n=2$ density-matrix element $\mathrm{Re}\,(\rho_{s0,p0})$ vs electron scattering angle for 200-eV incident electron energy. (b) $n=2$ $\mathrm{Im}\,(\rho_{s0,p0})$.

Another example of this feature is shown in the angular distribution of the $n=3$ quadrupole moment $\langle 3z^2 - r^2 \rangle$ and its time derivative $\langle d/dt(3z^2 - r^2) \rangle$ (see Fig. 13). Here again, the final-state interactions strongly affect the PT-odd quadrupole time derivative, as evidenced by the large effect when these interactions are turned off in the CTA model.

We present in Fig. 14 the angular distribution of $\rho_{p0,p1}$ with scattering angle θ for zero azimuthal angle, e.g., scattering in the x-z plane. The $\mathrm{Re}\{\rho_{p0,p1}\}$ is proportional to a quadrupole moment, whereas the $\mathrm{Im}\{\rho_{p0,p1}\}$ is proportional to the magnetic-dipole moment in the direction perpendicular to the scattering plane. These quantities are referred to as the alignment and orientation of the p states. In the PWBA $\mathrm{Im}\{\rho_{p0,p1}\}$ is identically zero. The DWBA goes through zero at about 40°, whereas

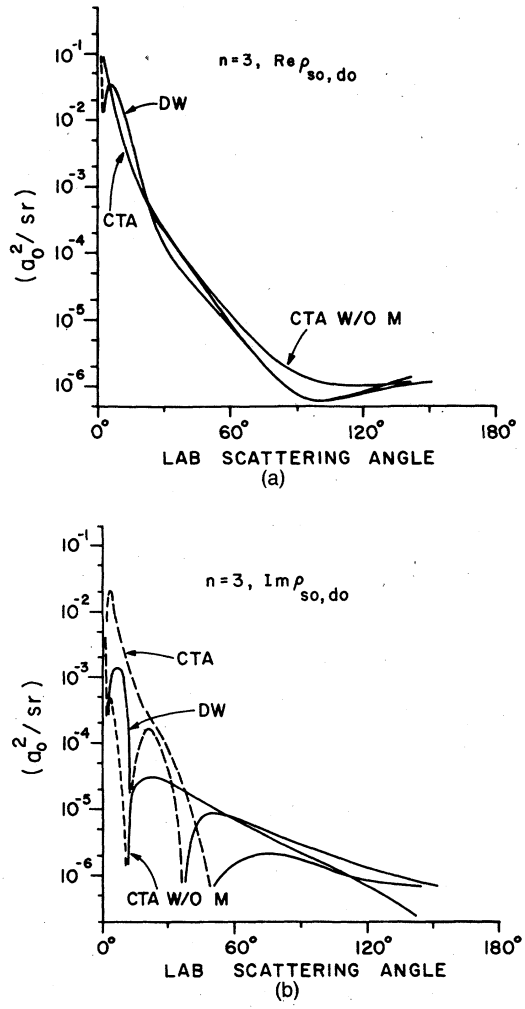

FIG. 13. Same as Fig. 12, except $n=3$ quadrupole moment and time-derivative moment $\rho_{s0,d0}$.

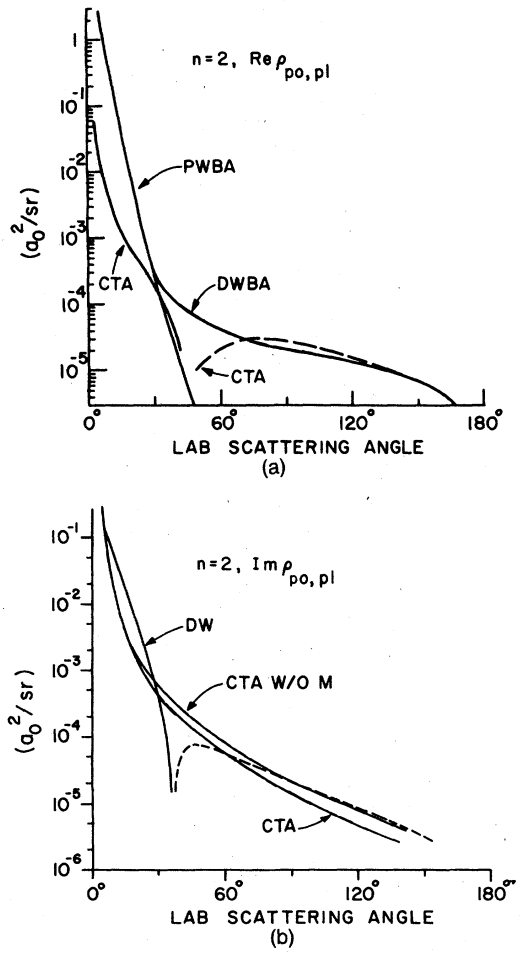

FIG. 14. Same as Fig. 12, except (a) $n=2$ quadrupole moment Re $\rho_{p0,p1}$ (b) $n=2$ magnetic dipole moment Im $\rho_{p0,p1}$.

the CTA (and the QCCA, to be presented elsewhere) has no sign reversal as a function of angle. Note that the mixing and distortion effects do not significantly effect the orientation, since the CTA results with and without these effects are similar. The alignment ($\mathrm{Re}\rho_{p0,p1}$) within the PWBA and DWBA are similar in the forward direction, but significantly different at larger angles. However, the CTA result has a change in sign at about 50° (the change of sign in the QCCA is at larger scattering angles), whereas the PWBA shows no such feature. The diffraction effects left out of the CTA and the other improvements of the QCCA will result in substantially changing the angular distribution.[14] In particular, small angle results are not reliable (since $\Delta M \neq 0$).

We have described some of the physical phenomena giving rise to the general trends observed. These include angular momentum barriers at low energies, the impulsive nature of the excitation from the ground state to the final state, the mixing and distortion of the nearly degenerate final states, and the importance of the interaction time for the final-state interactions. To emphasize these physical phenomena, we now describe them in a slightly different fashion.

The PWBA incorporates some aspects of the impulsive excitation process. As already mentioned, the only dynamical variable available in the PWBA is the momentum transfer $\vec{q}$, imparted to the bound electron. The nonvanishing PWBA multipole moments must therefore be constructed from this momentum-transfer vector. Thus the time rate of change of the PWBA z component of the dipole moment is proportional to $f_1(q^2)q_z$. The z component of the quadrupole moment is proportional to

$f_2(q^2)(3q_z^2 - q^2)$, etc. Figure 12 indicates that at 200-eV incident electron energy, the time rate of change of the $n=2$ dipole moment in the z direction is negative for all scattering angles [thus $f_1(q^2)$ is negative for the q^2 sampled]. Integrated over all scattering angles the PWBA $n=2$ quadrupole moment, $12[\sigma(2p1) - \sigma(2p0)]$, is positive. At 0° and at 180° $f_2(q^2)$ is positive (by symmetry arguments), but the functional dependence of $f_2(q^2)$ on q^2 is not determined by symmetry and must be computed.

For those multipole moments which vanish by PWBA symmetry arguments, the DWBA indicates the departures from the PWBA within an impulsive model incorporating the distortion of the scattered electron motion. These departures are illustrated dramatically in the angular distributions of the dipole moments $\mathrm{Re}\rho_{s0,p0}$, and the time rate of change of quadrupole moments $\mathrm{Im}\rho_{s0,d0}$, as obtained using these approximations. An understanding of these departures of DWBA, or CTA without coupling, from PWBA, and the departures of these approximations from the full CTA are in hand. In the DWBA, the PT-even multipole moments depend upon the distorted-wave phase shifts through the cosine of the differences of these *small* phase shifts, whereas the PT-odd multipole moments depend upon the sine of the phase shifts. The cosine of a small number depends upon the number only to second order, whereas the sine is linearly dependent upon the number and therefore much more sensitive. The inclusion of mixing and distortion changes the phases of the S-matrix elements, and since the PT-odd multipole moments depend upon the S-matrix phases through a sine function, their dependence upon mixing and distortion is much more drastic than the PT-even multipole moments.

The result of the distortion and mixing of the degenerate excited states produced in a collision that results from the long-range interaction of the scattered electron with the excited states can be understood on the basis of electrostatic arguments. At large distances $|\vec{R}|$ of the scattered electron from the atom, we can expand the potential energy of interaction V in the form

$$V(R) = \int [\delta(r) + \rho(r)] \frac{(-e)}{|\vec{r} - \vec{R}(t)|} d^3r$$
$$= \phi(R) Q^{\mathrm{atom}} + \vec{E}(R)\langle\vec{r}\rangle + \frac{1}{2}\sum_{ij}\left(\frac{\partial^2\phi}{\partial r_i \partial r_j}\right)_{r=0}\langle 3r_i r_j - r^2\rangle , \quad (3.8)$$

where

$$\phi(R) = \frac{-e}{R(t)} ,$$
$$\vec{E}(R) = \frac{e\vec{R}(t)}{R(t)^3} ,$$
$$\left(\frac{\partial^2\phi}{\partial r_i \partial r_j}\right)_{r=0} = \frac{3R_i R_j - R^2\delta_{ij}}{R^5} .$$

Since the atom is uncharged, the leading terms in this expansion are the dipole and quadrupole terms. This expansion for the potential energy of interaction of the scattered electron with a given particular excited-state manifold can be analyzed to qualitatively understand the effects of the mixing and distortions of the degenerate excited states of the particular excited-state manifold.

Let us consider the response of the bound-electron cloud to the (time-dependent) potential induced by the presence of the scattering electron (see Fig. 15). Consider the classical trajectory A of a sufficiently fast electron (sufficiently fast that a classical picture for the relative motion has some validity). The chances are that if the ground-state hydrogen atom is excited, this excitation will occur when the incident electron is close to the hydrogen atom. This region is indicated by the letter "a" in Fig. 15. Upon leaving the region "a", the bound and incident electrons will repel, inducing a dipole moment. An identical analysis can be performed for trajectory B. The net result for these trajectories, and for forward scattered trajectories in general, indicates that the long range contribution to $\langle z\rangle$ is negative and that $\langle \dot{z}\rangle$ due to the mixing is positive. A similar analysis shows that the long-range contribution to quadrupole moments $\langle 3z^2 - r^2\rangle$ are positive for trajectories which are forward scattered and that the contribution to the quadrupole moment time derivatives (for $n \geq 3$) $\mathrm{Im}\{\rho_{s0,d0}\}$ are negative. For the quadrupole moments these conclusions are true for backward-scattered trajectories also since the sign of R_z does not enter into $(\partial\phi/\partial r_i \partial r_j)_{r=0}$. As is clearly demonstrated by the $n=2$ dipole moment and the $n=3$ rate of change of

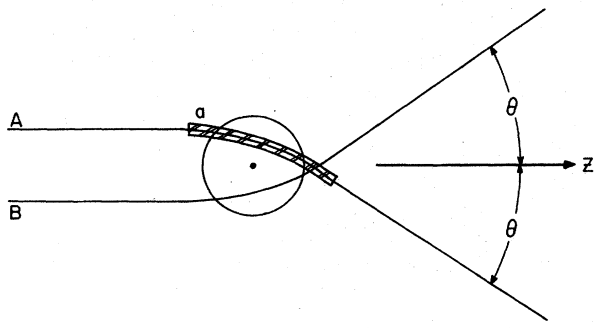

FIG. 15. Schematic representation of trajectories of electron scattering into scattering angle θ. Region a is where excitation of $n=2$ state is most likely for trajectory A.

quadrupole moment, the mixing and distortion effects are very important in considering some aspects of the collision.

IV. EXPERIMENTAL DETERMINATION OF COHERENCE MULTIPOLE MOMENTS

The coherence multipole moments can be determined experimentally by monitoring the radiation of the coherently excited states when they are subjected to external fields. The intensity of dipole radiation of polarization $\hat{\epsilon}$ from manifold f to manifold f' at time t after production of the excited state f manifold, in the presence of external $\vec{E}$ and $\vec{M}$ (time independent) fields is given by

$$I(\hat{\epsilon},\vec{E},\vec{M},t)=\mathrm{Tr}_{\{f'\}}\hat{\epsilon}\cdot\vec{r}\,U(t,0;\vec{E},\vec{M})\rho_f \times U^{\dagger}(t,0;\vec{E},\vec{M})\hat{\epsilon}^{*}\cdot\vec{r}\,. \tag{4.1}$$

Here ρ_f is the density matrix for manifold f at time zero. Actually, the collision-producing event for sufficiently fast electrons is effectively over 10^{-16} sec after the collision began, whereas the decay occurs in a time scale of about 10^{-8} sec. Therefore, we consider 10^{-16} sec as $t=0$. $U(t,0;\vec{E},\vec{M})$ is the evolution operator of the f manifold which described the precession of the states within the f manifold as well as the decay of this manifold. If we denote the (real and imaginary) components of the initial density matrix by $\{\rho_\nu\}$, the intensity of radiation is expressed in terms of these components by the sum

$$I(\hat{\epsilon},\vec{E},\vec{M},t)=\sum_\nu C_\nu(\hat{\epsilon},\vec{E},\vec{M},t)\rho_\nu\,, \tag{4.2}$$

where the coefficients C_ν are calculated by evaluating the trace in Eq. (4.1). The methods of calculating these coefficients for small, but arbitrary static fields are straightforward but tedious.

Consider as an example the following experiment. For incident electrons of a specified energy, measure the Balmer $\alpha(n=3$ to $n=2)$ radiation of given polarization $\hat{\epsilon}_x$ for light emitted along the y axis, in coincidence with an electron with 12-eV energy loss scattered by an angle θ in the x-z plane, in the presence of an external electric field $\vec{E}$ and magnetic field $\vec{M}$. The electron, *when it reaches the atom*, must have the specified energy and must be moving along the z direction. The intensity of radiation for this experiment is given by

$$I(\hat{\epsilon}_x,\vec{E},\vec{M})=\int_0^\infty dt\,\mathrm{Tr}_{\{n=2\}}\,\hat{\epsilon}_x\cdot\vec{r}\,U(t,0;\vec{E},\vec{M})\rho_{\{n=3\}} \times U^{\dagger}(t,0;\vec{E},\vec{M})\hat{\epsilon}_x\cdot\vec{r}\,. \tag{4.3}$$

The time dependence of the radiation is not measured. Here, $\rho_{\{n=3\}}$ is the projection onto $n=3$ of $\rho(E_e,\Omega_e)$, the density matrix for scattering into the specified scattering angle Ω_e.

Another, in fact simpler, experiment is to measure the same radiation intensity as above, but not in coincidence with the scattered electron. Except for cascading effects (the energy loss of the electron is not measured) the intensity of radiation is again given by (4.3), but $\rho_{\{n=3\}}$ is the angle averaged density matrix of the $n=3$ manifold. The beautiful experiment of Mahan and Smith[15] is this type of experiment, performed with zero magnetic field, with electric field along the z direction, and with unpolarized light detected. They measured the Balmer α radiation intensity for 200- and 500-eV incident electron energies as a function of electric field in the z direction. Krotkov first calculated the total intensity versus electric field strength using PWBA, but neglecting $\rho_{s0,d0}$ terms.[16]

With zero external fields the intensity of radiation is proportional (from Eq. 4.2) to the cross sections, σ_{3s}, σ_{3p0}, σ_{3p1}, σ_{3d0}, σ_{3d1}, σ_{3d2}, and one (complex) off-diagonal density matrix $\rho_{s0,d0}$. All other coefficients for the (nonvanishing) density-matrix elements ($\rho_{s0,p0}$, $\rho_{p0,d0}$, and $\rho_{p1,d1}$) vanish. Note that even at zero-field strength the intensity of radiation is proportional to an off-diagonal density-matrix element. With an arbitrary electric field along the z axis, the radiation intensity is proportional to all the above coherence multipole moments[17] with coefficients $\{C_\nu\}$, which are calculable from the evolution of the atomic states in the presence of the field. The coefficients $\{C_\nu\}$ do *not* in any way depend upon the *production* dynamics of the excited-state manifold. Unfortunately, for the $n=3$ states there are six cross sections and eight coherence parameters involved in the intensity of radiation for an arbitrary electric field. Given the intensity of radiation as a function of electric field E_z, and knowing the coefficients $\{C_\nu(E_z)=\int_0^\infty dt C_\nu(E_z,t)\}$, it is possible in principle to determine all the density-matrix elements. This task can be broken into more manageable parts by considering the symmetric and antisymmetric parts, of the intensity of radiation as a function of electric field.[17,18] The symmetric curve $I(E_z)+I(-E_z)$ is linear in the even-parity cross sections, and the quadrupole moment and its time derivative $\rho_{s0,d0}$, whereas the antisymmetric curve, $I(E_z)-I(E_z)$, is linear in the odd-parity dipole moments and dipole time derivatives ($\rho_{s0,p0}$, $\rho_{p0,d0}$, $\rho_{p1,d1}$).

Figure 16 plots the symmetric and antisymmetric $H\alpha$ intensity as a function of electric field for 200-eV incident electron energy as calculated with several scattering models and as obtained experimentally. The concavity of the experimental difference curve suggests that the dipole moments are comparable with the dipole-moment time derivatives, as predicted by our CTA calculations. However, the

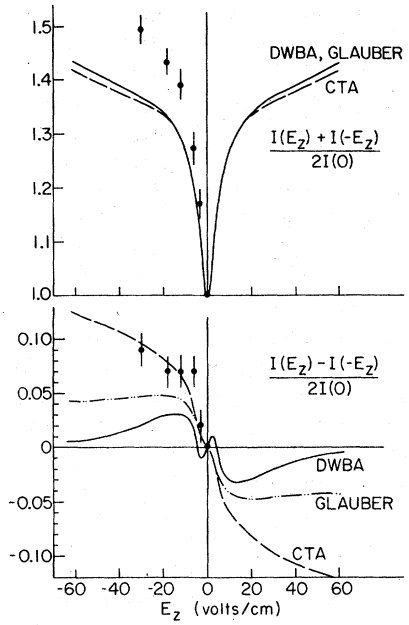

FIG. 16. Symmetric and antisymmetric H_α intensity vs applied external electric field for 200-eV electron impact energy. Data taken from Mahan and Smith (Ref. 15).

experimental symmetric curve is quite far from the theoretical predictions based upon any of the model calculations. The symmetric curve is most sensitive to the cross sections, and not very sensitive to the $\rho_{s0,d0}$ density-matrix element (since the coefficients C_ν of $\rho_{s0,d0}$ are small relative to the cross section coefficients). This discrepancy is at present unresolved.

V. CONCLUSION

We find that certain of the coherence multipole moments are extremely sensitive to the correlation of the bound electron and the incident electron. The study of the coherence multipoles is in fact the only way to extract some of this correlation information. These electron correlations are in some sense the same phenomena which give rise to the H^- bound state and doubly excited heliumlike systems,[19,20] but now studied at energies above the first continuum. These correlations give rise to large final-state interactions of the excited hydrogen states. The final state interactions between the bound and scattered electrons can *not* be treated by a perturbation expansion of the interaction between the scattered and bound electron. Even at 10-keV incident electron energy, when the velocity of the projectile electron is much greater than the velocity of the bound electron, a perturbation approach fails. Thus a PWBA or a DWBA is totally incapable of dealing with the collision dynamics (even at 10 keV) which we learn about from our study of some of the multipole moments. We present calculations which properly incorporate these dynamical effects. In particular, we find the PT-odd multipole moments the most sensitive to the details of the dynamics. The importance of the mixing of degenerate eigenstates and the distortion of these energy eigenstates by the incident electron have been demonstrated. The role of the angular momentum barriers at low energies, the impulsive nature of the excitation process at higher energies, the interaction time for the final state interactions, and the loss of flux to highly excited and ionized regions of the spectrum, have been pointed out.

In this paper we have dealt with the hydrogen atom originally in its ground state. Since the ground state is nondegenerate, no initial state interactions play a role. Clearly, in dealing with collisions of initially excited states, the strong long-range initial-state interactions between the degenerate initial states will play an important role. Extensive studies of this phenomena have yet to be carried out. Also, the role of the phenomena discussed above in electron charged-hydrogenic systems (i.e., e-He^+) has not been extensively studied.

It is the near degeneracy of the eigenstates with the same principal quantum number in hydrogenic systems which allow the detection of the mixed-l coherence multipole moments. In nonhydrogenic systems these mixed-l multipoles oscillate with a frequency too fast to allow their detection. However, application of carefully chosen time-independent and/or time-dependent fields may allow the determination of these coherence multipole moments for Rydberg states of atoms and molecules.

The study of coherence multipole moments of hydrogenic systems produced upon excitation by ion and atom collisions and upon charge transfer collisions will be of considerable help in the unraveling of the collision dynamics of such systems. Study of the mixed-l coherence multipoles of excited rotational states of diatomic and polyatomic systems may also be of interest.

I am grateful to G. Gabrielse for his full collaboration in both the calculational aspects and deducing the physical insights of the present work and to H. Gordon Berry for his continuous interest and encouragement. Work performed under the auspices of the Division of Basic Energy Sciences of the U. S. Department of Energy.

*Present address: Dept. of Chemistry, Ben-Gurion University of the Negev, Beer-Sheva, Israel.

[1]G. Gabrielse and Y. B. Band, Phys. Rev. Lett. 39, 697 (1977).

[2]A. Messiah, *Quantum Mechanics* (Wiley, New York, 1966), pp. 331–338; Roger G. Newton, *Scattering Theory of Waves and Particles* (McGraw-Hill, New York, 1966) pp. 222–231.

[3]G. Gabrielse (unpublished).

[4]U. Fano and J. H. Macek, Rev. Mod. Phys. 45, 53 (1973).

[5]K. Alder, A. Bohr, T. Huus, B. Mottelson, and A. Winter, Rev. Mod. Phys. 28, 432 (1956).

[6]J. A. Belling, J. Phys. B 1, 136 (1968).

[7]R. V. Calhoun, D. H. Madison, and W. N. Shelton, Phys. Rev. A 14, 1380 (1976); Phys. Rev. A 16 (1977).

[8]P. G. Burke and W. D. Robb, Adv. At. Mol. Phys. 11, 143 (1975); P. G. Burke, H. M. Shey, and K. Smith, Phys. Rev. 129, 1258 (1963).

[9]M. J. Seaton, J. Phys. B 7, 1817 (1974).

[10]E. Gerjuoy and B. K. Thomas, Rep. Prog. Phys. 37, 1345 (1974); W. Williamson, Jr. and G. Foster, Phys. Rev. A 11, 1472 (1975); J. N. Gau and J. Macek, Phys. Rev. A 12, 1760 (1975); C. J. Joachain and C. Quigg, Rev. Mod. Phys. 46, 279 (1974).

[11]F. T. Chan (private communication).

[12]K. W. Ford and J. A. Wheeler, Ann. Phys. (N. Y.) 7, 259, 287 (1959).

[13]Y. B. Band, J. Chem. Phys. 70, 4 (1979); Y. B. Band, J. Phys. B (in press).

[14]Y. B. Band (unpublished).

[15]A. H. Mahan and S. J. Smith, Phys. Rev. A 16, 1789 (1977).

[16]R. Krotkov, Phys. Rev. A 12, 1793 (1973).

[17]T. G. Eck, Phys. Rev. Lett. 31, 270 (1973).

[18]M. Lombardi, M. Giroud, and J. H. Macek, Phys. Rev. A 11, 1114 (1975).

[19]K. Frankowski and C. L. Pekeris, Phys. Rev. 146, 46 (1966).

[20]J. Macek, J. Phys. B 2, 831 (1968); C. D. Lin, Phys. Rev. A 12, 493 (1975).